Sensors & Actuators: B. Chemical 344 (2021) 130313

Contents lists available at ScienceDirect

Sensors and Actuators: B. Chemical

journal homepage: www.elsevier.com/locate/snb

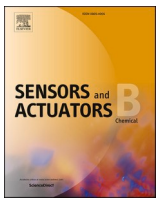

Amine-functionalized metal-organic framework ZIF-8 toward colorimetric CO_2 sensing in indoor air environment

Adrian K. Davey [a,b], Xiang Gao [a,b], Yong Xia [a,b], Zhou Li [a,b], Matthew N. Dods [a], Steven Delacruz [a,b], Aifei Pan [a,b], Sanket Swamy [a], David Gardner [a,b], Carlo Carraro [a,b], Roya Maboudian [a,b,*]

[a] Department of Chemical and Biomolecular Engineering, University of California, Berkeley, CA, 94720, USA
[b] Berkeley Sensor & Actuator Center, Berkeley, CA, 94720, USA

ARTICLE INFO

Keywords:
Metal-organic framework (MOF)
Zeolitic imidazolate framework (ZIF)
Colorimetric sensing
Zwitterion mechanism
Air quality monitoring
RGB value

ABSTRACT

Carbon dioxide (CO_2) has been shown to contribute to human health consequences indoors, such as shortness of breath, nasal and optic irritation, dizziness, and nausea. In this work, we explore the potential of metal–organic frameworks (MOFs) as highly-porous, crystalline sorbents for sensitive colorimetric CO_2 detection. In particular, the zeolitic imidazolate framework (ZIF-8) is chosen as the sorptive material due to its chemical stability and tunable CO_2 affinity. The colorimetric gas sensor is developed in methanol with three components: (i) MOF ZIF-8 as a high surface area adsorbent; (ii) ethylenediamine (ED) as the CO_2-affinitive basic function; and (iii) phenolsulfonpthalein (PSP) as the pH indicator. Colorimetric assays and ratiometric analysis confirm a colorimetric response to variable CO_2 concentrations of relevance to indoor air quality. The color response is attributed to a zwitterion mechanism whereby ED reacts with CO_2 to form a zwitterionic intermediate. This intermediate is then deprotonated by the pH indicator, shifting the pH and inducing a color change. Given its simple fabrication, rapid and obvious response, and stability in ambient environment, the ZIF-8-based colorimetric sensor provides a promising route for an improved indoor air quality monitoring.

1. Introduction

In recent decades, the design of airtight, energy-efficient buildings has resulted in homes and offices with lower rates of ventilation [1,2]. However, decreased ventilation rates in conventional buildings can result in elevated levels of indoor pollutants, which introduces health risks to building occupants [2]. Carbon dioxide (CO_2) is an odorless, colorless gas whose accumulation indoors imposes detrimental consequences on human health. The primary source of CO_2 indoors is attributed to building occupant metabolism [1], with minimum CO_2 concentrations of 400 ppm typically observed in offices [3]. However, with increased building occupancy and exacerbated ventilation conditions, indoor CO_2 levels can easily exceed 1000 ppm [3]. Thorough studies in the literature associate indoor climate variables (humidity, temperature, CO_2 concentration, and volatile organic compound concentration) with *sick building syndrome (SBS)*, which entails adverse health symptoms experienced indoors such as shortness of breath, optic and nasal irritation, tightness of the chest, dizziness, and fatigue [1,4,5]. Inside automobiles, previous research has reported the dangerous nature of elevated CO_2 levels as high as 3500 ppm, which are associated with compromised decision-making and drowsiness at the wheel [6]. Relatedly, the CO_2 permissible exposure limit (stipulated by the U.S. Occupational Health and Safety Administration) is set at 5000 ppm [7], which has been correlated with an increased diastolic blood pressure and mental effort to complete tasks, as well as an overall diminished personal wellbeing [1,8]. Higher CO_2 concentrations (above 10,000 ppm) can induce respiratory acidosis, rapid breathing, metabolic stress, and increased brain blood flow [1].

Given these precarious conditions for human health, various efforts have emerged toward development of CO_2 monitors for indoor deployment. The chief problem in gas sensing is the design of a sensor that is highly-sensitive to targeted species, energy-efficient, inexpensive to fabricate, stable, and convenient for users. Nondispersive infrared (NDIR) CO_2 sensors are popular commercial instruments that relate absorbed IR radiation to analyte concentration according to the Beer-Lambert law [9]. For CO_2 sensing, optical bandpass filters absorb IR

* Corresponding author at: Department of Chemical and Biomolecular Engineering, University of California, Berkeley, CA, 94720, USA.
E-mail address: maboudia@berkeley.edu (R. Maboudian).

https://doi.org/10.1016/j.snb.2021.130313
Received 20 April 2021; Received in revised form 11 June 2021; Accepted 15 June 2021
Available online 18 June 2021

wavelengths except the characteristic CO_2 absorption wavelength (4.26 μm) to minimize signal interference [9]. Advantages of the NDIR device include low limits of detection (< 100 ppm), high accuracy, and longevity (> 10 years) [9]. However, the CO_2 NDIR sensor has traditionally been challenged by power consumption and cost, as well as scalability limitations from necessary pathlengths (~cm) to enable ppm-level detection [9].

In contrast to the NDIR sensing technology, colorimetric sensing boasts several advantages, including easy preparation, user convenience, and obvious responses detectable by the human eye [10]. For example, the common colorimetric CO_2 sensor is developed based on a pH indicator and a lipophilic organic base in aqueous solutions [11,12]. When CO_2 is absorbed and reacts with the base, the indicator responds to the change in pH of the aqueous environment, thus triggering an immediate color change [11,12]. However, the solution-based colorimetric approach is limited by the handling and storage of the liquid phase and slow recovery kinetics [11]. For versatile colorimetric CO_2 sensing, porous, inexpensive, robust, and simply-synthesized solids are desired as the ideal sorbents and supports toward a reliable visual readout [11]. Some solid colorimetric devices, such as tertiary amino alcohols and dyes immobilized on porous γ-aluminum oxide supports [11], have been shown to exhibit a reversible colorimetric CO_2 response (at 500 ppm and up). In clinical settings, commercialized colorimetric CO_2 sensors loaded with Metacresol purple have been deployed for patient endotracheal tube placement, sensitive to CO_2 partial pressures of 5000 ppm (and up) [13,14]. Sol-gel matrices [15] and polymer-based sensing arrays [16] have been constructed to colorimetrically detect toxic gases in the atmosphere beyond CO_2, such as volatile organic compounds and SO_2.

Toward the realization of a prototypical gas sensor, we have investigated the potential of metal–organic frameworks (MOFs) as sorbents for indoor colorimetric CO_2 detection. MOFs are highly-porous, crystalline extended structures composed of metal clusters (or cations) coordinated to organic ligands [17–19]. Due to their structural and compositional tunability [20–23], MOFs offer a diverse array of functions, including gas separations and storage [24–27], chemical sensors [28–30], and heterogenous catalysis [31,32]. For this work, the zeolitic imidazolate framework (ZIF) is selected from MOF candidates. ZIFs are tetrahedrally-coordinated transition metal ions coordinated by imidazolate linkers; the metal-imidazolate-metal angle is similar to the 145° Si-O-Si angle in zeolites, which give these materials "zeolite-like" topologies [33]. Specifically, we identify ZIF-8, a well-studied MOF constructed from the linkage of zinc (Zn^{2+}) ions and imidazolate (mIm^{-}) ligands [34]. ZIF-8 contains 3.4 Å six-member pore apertures and 11.6 Å pore cavities accessible for CO_2 adsorption [35]. Furthermore, several theoretical and computational studies [36–38] have shown preferential CO_2 adsorption sites associated with the organic linker. ZIF-8 also exhibits notable structural flexibility [39–42], as well as a high thermal and chemical stability [43–45]. In recent studies, MOF-based sensors have been reported to detect CO_2 levels relevant to indoor quality using chemiresistive techniques [29] and electrochemical impedance spectroscopy [46], both requiring external power for their operations. On the other hand, the sensor presented here, based on colorimetry, exhibits an obvious color change to the human eye, and hence is passive.

Colorimetry is employed here as the transduction mechanism to develop a MOF-based device whose CO_2 affinity is of interest to indoor environment. In our study, the MOF-based colorimetric CO_2 sensor, referred to as PSP-ED/ZIF-8, is developed from three components: (a) the adsorbent, ZIF-8; (b) the basic primary amine, ethylenediamine; and (c) the pH indicator, phenolsulfonpthalein. Given the wide range of CO_2 levels that humans can experience within homes, offices, and vehicles [1,6,7], the prototype is exposed to 700 – 7500 ppm CO_2 in variable humidity. Across this span of CO_2 concentrations, highly-reproducible red-green-blue (RGB) intensities developed from smartphone video are used to quantify the colorimetric response. Furthermore, the interplay of ZIF-8, ethylenediamine, and phenolsulfonpthalein toward colorimetric CO_2 detection is discussed, as well as future endeavors toward comprehension of water suppression of sensing behavior.

2. Materials and methods

2.1. Synthesis of the PSP-ED/ZIF-8

PSP-ED/ZIF-8 synthesis follows a modified procedure adapted from Cravillon et al. [47]. 1.04 g of zinc nitrate hexahydrate [$Zn(NO_3)_2{\cdot}6H_2O$; Fischer Scientific] and 1.04 g of 2-methylimidazole (Hmim, 99 %, Sigma-Aldrich) are dissolved in 60 mL of methanol (Fischer Chemical), separately, and then mixed and allowed to react at room temperature overnight (with no stirring). Pristine ZIF-8 crystals are then partially activated, washing three times with methanol using a Beckman Coulter, Inc. Microfuge®18 Centrifuge at 12,000 rpm for 5-min. For characterizing the pristine ZIF-8, the washed ZIF-8 crystals are dried at 60 °C on a hot plate overnight. Then, the ZIF-8 crystals are recovered, placed in an oven, and heated at 110 °C (in air) for 24 h.

For the synthesis of PSP-ED/ZIF-8 material, a 2 % ethylenediamine (99 %, Sigma-Aldrich) solution (% v/v) in methanol is produced by adding 400 μl of ethylenediamine to 19.6 mL of methanol. 10 mg of phenolsulfonpthalein (Acros Organics) are then dissolved into this solution. Aliquots of this solution are then mixed with the partially-activated ZIF-8 (80 mg ZIF-8/mL colorimetric solvent) with prolonged sonication to achieve the PSP-ED/ZIF-8 solution. Optical images of the material at various stages of synthesis are depicted in Fig. S1.

2.2. Material characterization methods

Powder X-ray diffraction (PXRD) patterns are collected with a Bruker diffractometer (Cu K-α radiation, λ = 1.54 Å, 40 kV, 40 mA). Nitrogen adsorption isotherms are measured at 77 K using Tristar II 3020 volumetric adsorption analyzers manufactured by Micromeritics (Norcross, GA). Before adsorption measurements, the samples are out-gassed under vacuum for 24 h at 150 °C. The specific surface area of the samples is calculated using the Brunauer–Emmett–Teller (BET) method within the relative pressure range of 0.01 to 0.95 (p/p_0). Sample particle size is acquired using scanning electron microscopy (SEM, Hitachi S-5000). A thin Au/Pd layer is sputter deposited on the samples to afford some electrical conductivity to the material prior to SEM imaging.

2.3. Gas sensing characterization

Quantitative assessment of colorimetric CO_2 sensing is accomplished through ex-situ ultraviolet-visible diffuse reflectance spectroscopy with a Cary 5000 (Instrument No. 5.2) spectrophotometer at a scan rate of 600 nm/min. The Kubelka-Munk transform, F(R), shown as Eq. 1, is a two-flux model that relates the material's diffuse reflectance (R) to an absorption coefficient (K) and scattering coefficient (S), which depends on several parameters such as particle size and loading [48–53].

$$F(R) = \frac{(1-R)^2}{2R} = \frac{K}{S} \tag{1}$$

Colorimetric sensing experiments using UV–vis spectroscopy are conducted as follows. Cellulose filter paper (VWR North American) is first cut into a 0.7cm × 0.7cm square, affixed to a piece of double-sided black tape of same size, placed inside the UV–vis sample enclosure, and used as a blank in the UV–vis spectrophotometer. Then, another cellulose filter paper of the same size is cut and 15 μl of PSP-ED/ZIF-8 solution is drop-cast on it. After 120 s sitting in ambient environment, most of the methanol evaporates. This coated paper is similarly placed in the spectrophotometer and a "Pre-CO_2 exposure" plot of reflectance (% R) vs wavelength (nm) is recorded.

After this run, the sample enclosure is partially opened and placed inside a specifically designed plexiglass enclosure (9cm × 7.4cm × 3.6 cm). Colorimetric CO_2 uptake in variable humidity is achieved by

connecting the enclosure to a gas manifold (Fig. S2), which allows computer-controlled delivery of CO_2 and relative humidity via mass flow controllers (Bronkhorst) set by LabView software. A cylinder of 22,000 ppm CO_2 balanced in nitrogen is used (Praxair). Purge and balance streams are provided by passing house air through pressure swing adsorption dryers to remove humidity and an activated carbon scrubber to eliminate contaminants. Different humidity levels are created via a bubbler and controlled by the same feedback calibration system set by the LabView program. A wireless GasLab Plus CM-501 NDIR sensor is integrated in the apparatus to calibrate the achieved CO_2 and humidity levels set in LabView (as shown in Fig. S3). For the measurements reported here, the total gas flow rate is kept constant at 300 standard cubic centimeters per minute (sccm) and the flow stream temperatures are measured at room temperature (22.0 ± 0.5 °C).

For a given trial, the system is first purged with dry air until < 500 ppm CO_2 and the desired humidity are achieved. Then, the sample is exposed to the desired CO_2 concentration while the NDIR sensor logs the data until steady state is reached. The sample enclosure is then placed back in the spectrometer and UV–vis spectra are collected. For each trial, the % R data are converted to F(R) values (using Eq. 1) and plotted. In typical absorbance spectra, phenolsulfonpthalein exhibits a color change from purple (λ_{max} = 570 nm) in basic environment to yellow (λ_{max} = 443 nm) in acidic environments [54]. For each CO_2 exposure (dry or humid), the ratios of the F(R) values at 443 and 570 nm are computed and plotted against CO_2 concentration (ppm). For each CO_2 exposure, at least two trials are averaged, and the standard deviation is depicted as error bars.

Optical images of the samples under various environments are also obtained using the direct exposure technique (all exposures at 300 sccm). For direct exposure measurements, colorimetric ZIF-8 sensors are drop-cast on cellulose filter paper and allowed to dry for 120 s in ambient environment. Then, a video (using a Google Pixel smartphone) is recorded with applied CO_2 and relative humidity (for 10 s). After 10 s, the CO_2 atmosphere is removed, and the sensor recovers over 15 s intervals before subsequent exposure. Background CO_2 and relative humidity are logged with the GasLab Plus CM-501 CO_2 NDIR sensor.

RGB values are extracted from optical images (captured via Google Pixel smartphone) using MATLAB software. Each image is read into the MATLAB script as a 1.3" × 1.3" square and outputted as a 125 × 125-pixel RGB distribution. RGB values range from 0 to 255, where 0 corresponds to minimal intensity and 255 maximum intensity of visible light. Absolute yellow, for example, would have a RGB value of (255, 255, 0), whereas absolute purple would be (255, 0, 255). Because the center of the drop-cast PSP-ED/ZIF-8 is exposed using the direct exposure method, RGB values are obtained with the Y-axis held constant at 62 pixels, with the X-axis ranging from 60 to 80 pixels. Mean RGB values (and standard deviations) for variable CO_2 concentration and relative humidity are computed using OriginPro software and tabulated.

3. Results and discussion

3.1. Material characterization

Fig. 1 displays the XRD patterns obtained on the as-synthesized pristine ZIF-8, the PSP-ED/ZIF-8, as well as the simulated ZIF-8 (refcode: VELVOY) [55]. The major characteristic diffraction peaks at 2θ = 7.3, 10.4, 12.6, 14.6, 16.4, 17.9, 22.0, 24.4, and 26.6° associated with the (011), (002), (112), (022), (013), (222), (114), (233), and (134) planes are observed [56]. These results are consistent with prior reports of the pristine MOF developed in methanol at room temperature, indicating formation of the expected sodalite structure [56]. The PSP-ED/ZIF-8 sensor stability is assessed using XRD (Fig. S4). Over a 4-week timespan (at room temperature), the bulk PSP-ED/ZIF-8 material retains its crystallinity in ambient environment, demonstrating no loss of the structural integrity of ZIF-8 when mixed with phenolsulfonpthalein and ethylenediamine in methanol. MOF structural

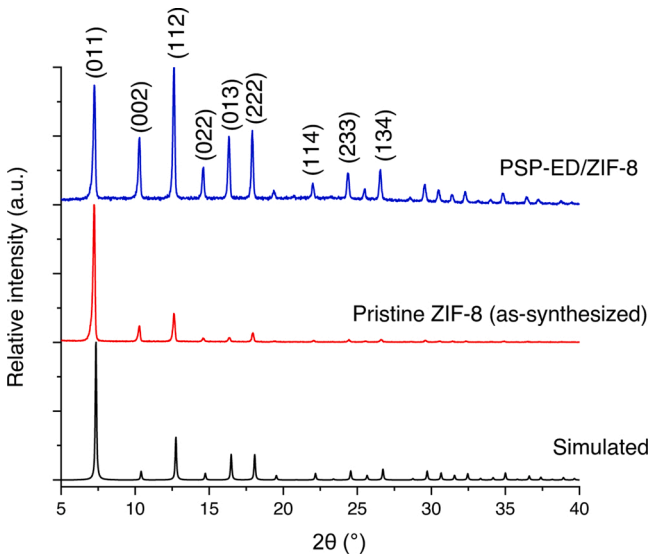

Fig. 1. Powder X-ray diffraction patterns (Cu K-α radiation, λ = 1.54 Å).

resistance to environmental factors, such as moisture and basicity, is imperative toward feasible use under various conditions [57]. In accordance with the Pearson acid-base concept, the strength of the soft ligand (imidazole) and soft metal (Zn^{2+}) interaction offers ZIF-8 a high chemical stability [58].

Representative SEM images of pristine ZIF-8 (washed) and PSP-ED/ZIF-8 are shown in Fig. 2. With the MOF precursor molar ratio used (metal: linker: solvent – 1:3.62:847) at room temperature in methanol, ZIF-8 nanocrystals (consistent in size with reported values in the literature) are obtained [59]. For the activated pristine ZIF-8, the BET surface area (calculated from the nitrogen isotherm in Fig. S5) is measured to be 1485 m^2/g, which is likewise in agreement with previously reported values [60,61].

3.2. Colorimetric analyses in dry environment

Representative colorimetric images of fresh PSP-ED/ZIF-8 exposed to CO_2 (dry) using the direct-exposure technique are shown in Fig. 3. With increased CO_2 exposure, the drop-cast PSP-ED/ZIF-8 (initially purple) demonstrates an obvious color shift to higher intensities of yellow. This colorimetric shift is rendered possible through collaboration of phenolsulfonpthalein, ethylenediamine, and ZIF-8. To highlight the critical role of all three components, the colorimetric responses to just phenolsulfonpthalein, phenolsulfonpthalein/ethylenediamine, and phenolsulfonpthalein/ZIF-8 materials are compared to PSP-ED/ZIF-8. As can be seen in Fig. 3A, all three components — ZIF-8, ethylenediamine, and phenolsulfonpthalein — are necessary to achieve a visible response. Without any of these components, the sensors exhibit no visible response to even high levels of CO_2.

Average RGB values for PSP-ED/ZIF-8 exposed to dry CO_2 are shown in Table S1, respectively. As observed in Fig. 3B, the degree of yellow achieved intensifies as the CO_2 concentration exposed increases from 700 to 7500 ppm. In accordance with these colorimetric results, the mean G-value increases with increasing dry CO_2 concentration, whereas the mean B-value decreases. While the R-values corresponding to dry CO_2 exposure do not exhibit a particular trend, the more drastic and consistent rise in green intensities and decrease in blue intensities indicate a stronger yellow color with increasing dry CO_2 concentration.

In addition to CO_2, volatile organic compound (VOC) and carbon monoxide (CO) exposure is linked to the development of specific human health symptoms indoors [2]. VOCs (such as acetone)—which are commonly released from aerosols, cleansers, and related household products—are associated with nasal, throat, and eye irritation [62,63].

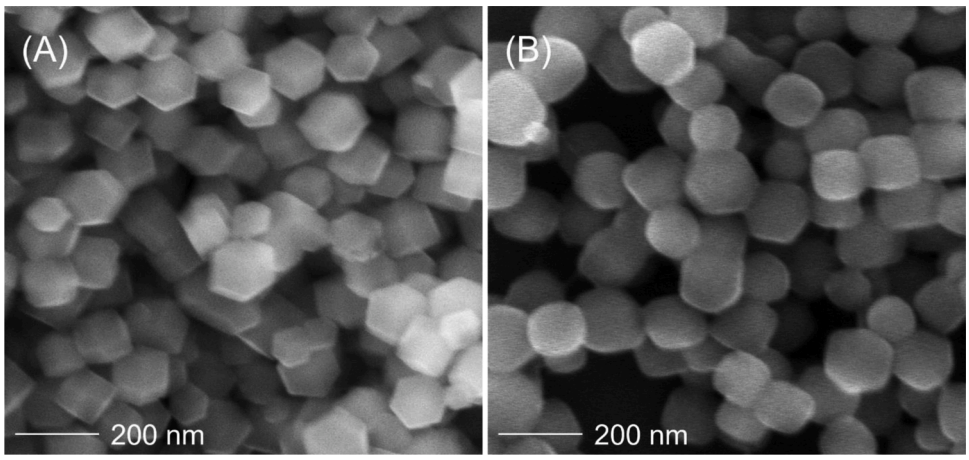

Fig. 2. SEM images for **(A)** washed pristine ZIF-8 and **(B)** PSP-ED/ZIF-8 (2% ED). Size bar =200 nm.

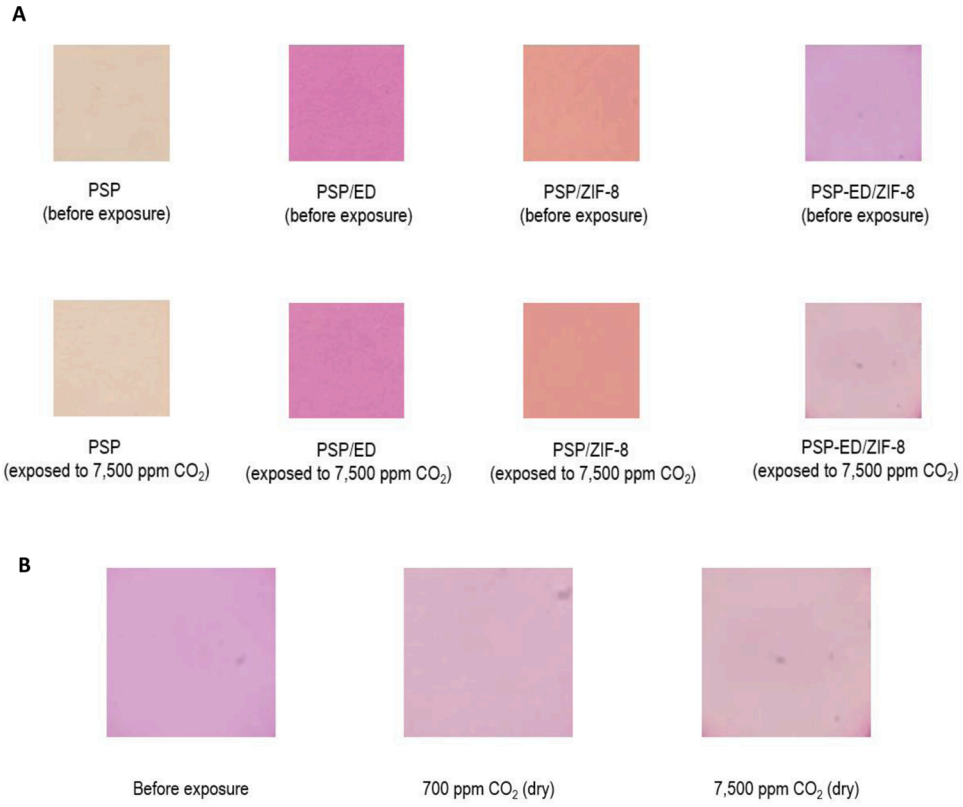

Fig. 3. (A) Effects of various components in colorimetric response to 7500 ppm CO_2. First column: 15 μL of a methanolic 0.5 mg/mL phenolsulfonpthalein solution drop-cast on cellulose filter paper. Second column: 15 μL of a methanolic 0.5 mg/mL phenolsulfonpthalein /ethylenediamine solution (2% ED, %v/v) drop-cast on cellulose filter paper. Third column: 15 μL of an 80 mg/mL ZIF-8 solution (prepared from a methanolic 0.5 mg/mL phenolsulfonpthalein solution) drop-cast on cellulose filter paper. Fourth column: 15 μL of PSP-ED/ZIF-8 drop-cast on cellulose filter paper. **(B)** Colorimetric response of PSP-ED/ZIF-8 before CO_2 is applied, when 700 ppm CO_2 is applied, and when 7500 ppm CO_2 is applied. All under dry conditions.

Similarly, fatigue is frequently observed with exposure to CO indoors [64]. Fig. 4 compares the response of PSP-ED/ZIF-8 to CO_2 (in dry house air), dry house air, acetone (in dry house air), and CO (in dry house air), all flowing at 300 sccm. Whereas an obvious yellow color change occurs in the presence of CO_2, the sensitivity of PSP-ED/ZIF-8 to both 200 ppm acetone and CO is significantly lower. However, compared to the freshly drop-cast PSP-ED/ZIF-8, a slight color change is observed in the dry acetone and CO exposures, which is attributed to the trace CO_2 present

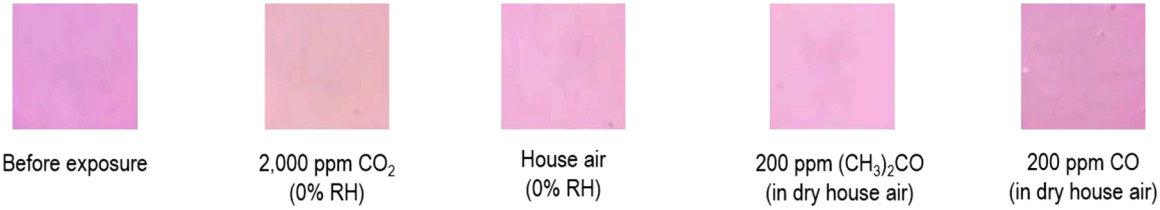

Fig. 4. PSP-ED/ZIF-8 profiles before target gas exposure; exposed to 2000 ppm carbon dioxide (dry); dry house air; 200 ppm acetone (in dry air); and 200 ppm carbon monoxide (in dry air).

in the balance house air (373 ± 2 ppm). Given the poor response to acetone and CO even at elevated levels (whereas their usual concentrations in indoor air are < 10 ppb [63] and < 30 ppm [64], respectively), the PSP-ED/ZIF-8 sensor exhibits a strong affinity for CO_2 compared to these indoor pollutants in dry atmosphere.

For the low partial pressures of CO_2 involved in this study, the visible change in colorimetric response to variable CO_2 concentrations can be difficult to qualitatively distinguish by human eye. In a similar manner to published work involving phenolsulfonpthalein absorbance spectra in cell culture media [65], plots of the 443/570 nm F(R) ratios from the UV–vis data are developed for each sensor at a specific humidity to draw quantifiable differences. First, F(R) vs. wavelength (nm) plots are collected (shown in Fig. 5). With increasing the concentration of CO_2, the exposed sensor becomes more yellow and the F(R) value at 570 nm decreases.

Ratiometric profiles from ex-situ diffuse reflectance UV–vis measurements are shown in Fig. 6 for the PSP-ED/ZIF-8 sensor. For this sensor, a broad range of target concentrations (700 – 7500 ppm CO_2) is tested. With increasing CO_2 concentration, the colorimetric ratios (red symbols) noticeably rise from 0.283 to 0.701 ratiometric units, and the corresponding colorimetric CO_2 response visibly intensifies from 700 to 7500 ppm CO_2 exposures under 0% relative humidity.

The observed colorimetric behavior is consistent with proposed reactions between ethylenediamine, CO_2, and other bases. In previous work, ethylenediamine has been grafted onto ZIF-8 via post-synthetic modification to provide basic sites toward an enhanced, solid-state CO_2 adsorption [66]. For the reported colorimetric analyte studies, the observed CO_2 response (in methanol) is proposed to occur via a two-step zwitterion mechanism [67–72], whereby (in this instance) CO_2 is adsorbed on ZIF-8 to react with the other colorimetric sensor components. In aqueous and nonaqueous solvents, ethylenediamine and CO_2 react (Eq. 2) to form a 1°,3°-zwitterion intermediate, RH_2N^+—COO^-:

$$CO_2 + RNH_2 \leftrightarrow RN^+H_2CO_2^- \quad (2)$$

The 1°,3°-zwitterion is then deprotonated (Eq. 3) by a base, B, which could be unreacted ethylenediamine, H_2O, solvent molecules, or other species in the system [67–72]. When phenolsulfonpthalein (pKa: 7.9) participates as the base, the deprotonation step shifts the pH from above 8.2 to below 6.8 and induces a colorimetric response from fuchsia to yellow [73].

$$RN^+H_2CO_2^- + B \leftrightarrow RNHCO_2^- + BH^+ \quad (3)$$

Repeat exposures at 700, 3,000, and 7500 ppm CO_2 (dry) are depicted in Fig. S6. The colorimetric CO_2 response occurs within seconds as the CO_2 concentrations are repeatedly introduced and removed. However, partial recovery is obtained with each sensor, as the final color after a third dry CO_2 exposure is modestly more yellow than that of the fresh sensor prior to dosage. While some solid-state MOF sensors demonstrate reversible CO_2 detection [74], amine-based liquid gas sensors can suffer from sluggish kinetics [11]. As shown in Eq. 3, the carbamates formed upon zwitterionic deprotonation in protic solvent are thermodynamically stable, requiring thermal regeneration processes to reuse the sensor [11]. Thus, the sensor presented here is envisioned as a single-use sensor for colorimetric CO_2 sensing, which is commensurate with modern acid-base commercialized colorimetric sensors implemented in hospital care [13].

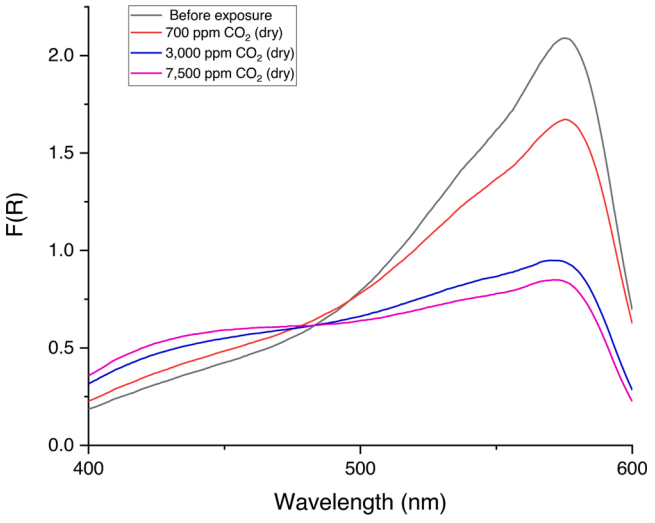

Fig. 5. F(R) vs wavelength (nm) profiles with PSP-ED/ZIF-8 in variable dry CO_2 environment.

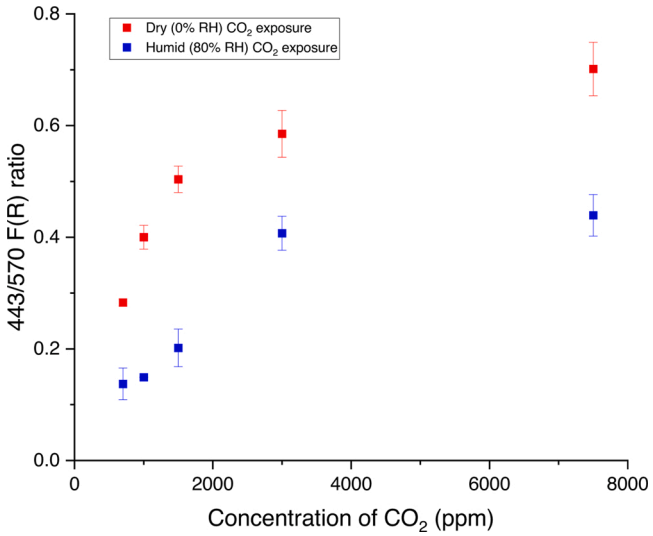

Fig. 6. UV–vis ratiometric profiles (700-7500 ppm CO_2) of PSP-ED/ZIF-8 in variable humidity.

As shown in Fig. 3, the combined interaction of phenolsulfonpthalein, ethylenediamine, and ZIF-8 with CO_2 facilitates colorimetric gas detection. Based on the BET measurements with the pristine MOF, ZIF-8 is expected to provide a high surface area for CO_2 adsorption, as well as accommodate both phenolsulfonpthalein and ethylenediamine for the two-step zwitterion reaction. Amine scrubbers (loaded with aqueous alkanolamines) are typically employed in CO_2 capture, whereby CO_2 absorption can be represented via film theory: CO_2 first diffuses from the bulk gas phase to the gas-liquid interface, then diffuses into the bulk liquid phase, and finally reacts with the amine via the zwitterion mechanism [75,76]. However, in the absence of ZIF-8, the cellulose filter paper absorbs methanol, phenolsulfonpthalein, and ethylenediamine, preventing a finite layer with enough thickness to perform the physical and chemical CO_2 absorption steps associated with amine chemistry. Finally, the absence of ethylenediamine (with either phenolsulfonpthalein dissolved in methanol or phenolsulfonpthalein and ZIF-8 mixed in methanol) precludes the formation of the zwitterion, which is necessary for deprotonation by the dye. Thus, it is apparent that the interactive chemistry of ZIF-8, phenolsulfonpthalein, and ethylenediamine generate a color change upon CO_2 adsorption.

Despite its decades of implementation, however, the validity of the zwitterion mechanism remains contested in the literature [77]. Ben Said et al. [78] performed density functional theory calculations that associated the development of the 1°,3°-zwitterion with high activation energy barriers and concluded this mechanism improbable. In addition, da Silva and Svendsen [79] used Hartree-Fock computational methods to study the mechanisms for reaction between CO_2 and aqueous alkanolamines. Their *ab initio* results suggested that a 1°,3°-zwitterion with a significant lifetime was unlikely [79]. Several authors have instead raised the single-step termolecular mechanism [77,79–81] as an

alternative reactive pathway, whereby an amine species reacts with one molecule of CO_2 and one molecule of base, B, according to Eq. 4. The termolecular reaction mechanism has been shown consistent with the reaction kinetics of CO_2 and several amines, such as monoethanolamine (MEA), aminoethylethanolamine, and diethylenetriamine [81].

$$CO_2 + RNH_2 \cdots B \leftrightarrow RNHCO_2^- + BH^+ \quad (4)$$

Formation of the 1°,3°-zwitterion, however, has been supported in some other reports. Xie et al. [82] simulated an aqueous CO_2-MEA system using a conductor-like polarizable continuum model and *ab initio* quantum mechanics/molecular mechanics. In contrast with prior authors, they posit that a two-step mechanism with a 1°,3°-zwitterion intermediate is a favorable reaction path [82]. Given the ongoing debate in the literature, it is difficult to precisely ascertain the reactive chemistry between adsorbed CO_2 and ED. However, due to its widespread use in aqueous and nonaqueous CO_2-amine systems, the zwitterion mechanism is situated in this work.

3.3. Colorimetric analyses in humid environment

The effect of ambient humidity on the colorimetric response of PSP-ED/ZIF-8 is also investigated. Representative colorimetric images for PSP-ED/ZIF-8 exposed 1500 ppm CO_2 at various humidity are provided in Fig. 7. While under dry conditions, the sensor responds quickly and obviously, the colorimetric sensor exhibits a suppressed response to CO_2 with incremented humidity.

The RGB mean values (shown in Table S2) demonstrate a reduced colorimetric CO_2 response in humid environment. With increased humidity, the R- and B-values increase, whereas the G-values generally decrease, leading to a diminished color change.

With increasing the concentration of CO_2, the suppressive effect of humidity remains apparent. RGB and ratiometric UV–vis profiles for 700, 3,000, and 7500 ppm CO_2 doses also reflect weaker colorimetric CO_2 responses upon 80 % RH exposure. As shown in Table S3, once 80 % RH is introduced, the green intensities decrease, and the blue intensities increase for all humid CO_2 concentrations compared to their dry values. The R-values for humid CO_2 exposure are higher than those upon dry CO_2 exposure. This combined decrease in G-values (and increase in R- and B-values) correspond to a less yellow color, indicating a suppressed CO_2 response. Similarly, as depicted in Fig. 6 and Table S4, the 443/570 nm F(R) ratios for humid CO_2 exposure are lower than those of dry exposure.

The exact mechanism of water interference in the colorimetric CO_2 sensing dynamics remains unclear. Differences in chemisorptive behavior in dry and humid environment have been observed in MOF studies. Flaig et al. [83] used solid-state ^{13}C cross-polarization magic angle spinning nuclear magnetic resonance spectroscopy to characterize CO_2 chemisorption in a diamine-functionalized IR-MOF-74-III. In dry environment, carbamic acid formation is observed from one amine reacting with CO_2 [83]. However, humidified (95 % RH) conditions converted CO_2 into ammonium carbamates upon reaction with two amines [83].

Under humid conditions, as seen with diamine-functionalized-IR-MOF-III, it is possible that the reaction stoichiometry of the colorimetric CO_2 sensing mechanism has altered toward a reduced CO_2 capacity. Assuming a pseudo steady-state hypothesis on the zwitterion intermediate concentration, the rate of reaction between CO_2 and primary amines (such as ethylenediamine) in aqueous (or nonaqueous) solvents can be approximated by Eq. 5 [84]

$$R_{CO_2} = \frac{-k_2\{CO_2\}[RNH_2]}{\frac{k_{-1}}{\sum k_B[B]} + 1} \quad (5)$$

where k_2 is the forward rate of reaction of CO_2 and ethylenediamine (Eq. 2), k_{-1} is reverse rate of reaction of CO_2 and ED (Eq. 2), and $\Sigma k_B[B]$ is the summation of bases present in the system eligible to deprotonate the zwitterion (Eq. 3) [84].

Under the first asymptotic limit, $\frac{k_{-1}}{\sum k_B[B]} << 1$ and deprotonation occurs much more rapidly compared to the reverse reaction in Eq. 2 [84,85]. The simplified rate law is first order with respect to CO_2 and primary amine, which has been found experimentally for aqueous CO_2-MEA systems at 303 K [84–87] and CO_2-ED systems in methanol at 303 K [69]. At the other asymptotic limit, $\frac{k_{-1}}{\sum k_B[B]} >> 1$ [84,85]. When a primary amine (such as ethylenediamine) contributes most to zwitterion deprotonation, Eq. 5 becomes second-order with respect to the amine [84,85]. The second asymptotic limit recovers the termolecular kinetics associated with Eq. 4, which Aboudheir et al. [88] showed for high CO_2-loaded (0.1−0.49 mol/mol), concentrated (3–9 M) aqueous MEA systems between 293 and 333 K.

Between these asymptotic limits, fractional reaction orders can be observed, as shown experimentally with CO_2-ED systems in pure and aqueous ethylene glycol solutions [69]. However, while such stoichiometric changes have been observed in amine-CO_2 systems, it is uncertain how the presence of ZIF-8 and phenolsulfonpthalein alters the reaction kinetics. Toward elucidation of the mechanistic colorimetric sensing mechanism between CO_2, ZIF-8, phenolsulfonpthalein, ethylenediamine, and potential interferants (such as H_2O), kinetic studies are required in methanolic solvent, which future studies will aim to provide.

Despite the characteristic water resistance of ZIF-8 from the methyl groups associated with its ligands and coordinatively saturated Zn^{2+} sites [43,89], ZIFs can show favorable H_2O adsorption isotherms through incorporation of hydrophilic moieties. Notably, ZIF-90 and SIM-1 display significant H_2O adsorption at 298 K compared to ZIF-8 due to the hydrophilic functional groups associated with their linkers, imidazole-2-carboxaldehyde and 4-methylimidazole-5-carbaldehyde [90]. In other work, amine-functionalized solid-state ZIF-8 (from toluene reflux) was shown to exhibit a 1–2 % suppression of CO_2 adsorption under the presence of preadsorbed water (10 % RH) [91]. In this context, we suspect that hydrophilic interactions between ethylenediamine and H_2O molecules could promote H_2O adsorption [92] and, under humid environment, disrupt the colorimetric CO_2 adsorption achieved in dry environment.

Alongside hydrogen bonding interactions between ethylenediamine and H_2O, the participation of H_2O in the zwitterion mechanism is another possible source of interference in the colorimetric CO_2 sensing. When hydrophilic ethylenediamine molecules are exposed to humid CO_2, the attracted H_2O molecules could engage in the second step of the

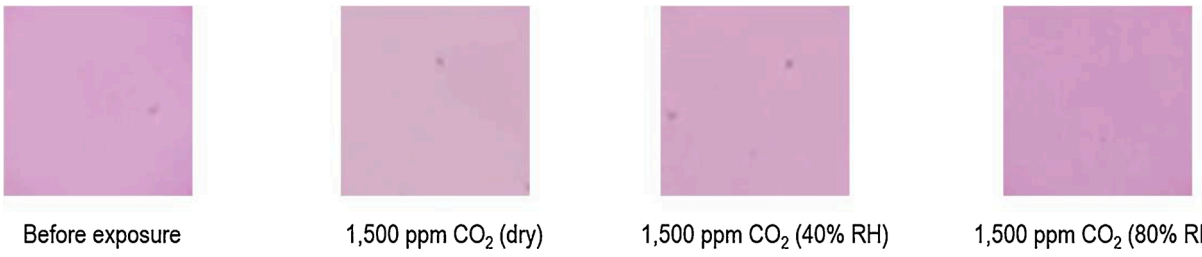

Fig. 7. Fresh exposure of PSP-ED/ZIF-8 to 1500 ppm CO_2 in dry environment, 40 % RH, and 80 % RH.

zwitterion mechanism and deprotonate the intermediate species [92]. The presence of hydrophilic ethylenediamine groups, then, could promote water adsorption, which subsequently introduces competition with phenolsulfonpthalein for deprotonation of the zwitterion and affects the apparent color [92].

Humid interference remains a challenge in colorimetric analyte detection using various materials [93,94]. Because humidity can disrupt colorimetric sensing through physical adsorption or chemical interactions, corrective measures can be difficult to precisely accomplish [94]. Toward addressing the effects of humidity on sensing performance, desiccants have been employed, as well as water-insoluble dyes compatible with hydrophobic substrates (such as polyvinylidene difluoride) [94]. The chemical tunability of MOFs can also be manipulated to enhance hydrophobic character. Using a post-synthetic shell--ligand exchange reaction (SLER), Liu et al. [95] substituted the outermost shell of ZIF-8 particles with 5,6-dimethylbenzimidazole and achieved an improved water-resistance and water stability. Thus, we remain optimistic in achieving a MOF colorimetric sensor with water-repelling attributes suitable for accurate detection of indoor chemical species.

4. Conclusions

In this work, we have designed and characterized a simple, chemically-stable, methanolic MOF-based colorimetric sensor toward detection of low CO_2 partial pressures of interest in indoor air quality monitoring. Colorimetric images, RGB values, and UV–vis spectroscopic studies show that PSP-ED/ZIF-8 is sensitive to CO_2 concentrations typical of indoor air in dry environment, with a lower limit of detection below 1000 ppm CO_2.

Despite an excellent response to CO_2 in dry environment, PSP-ED/ZIF-8 suffers in the presence of humidity. Both qualitative colorimetric images and quantitative UV–vis ratiometric profiles indicate colorimetric reduction upon exposure to humid CO_2. Here, the hydrophilic nature of ethylenediamine is expected to facilitate H_2O adsorption onto ZIF-8 and thus interfere with the visible CO_2 colorimetric detection otherwise achieved in dry environment. Competition between phenolsulfonpthalein and H_2O for zwitterion deprotonation is also considered as a possible source of suppression of the colorimetric CO_2 response. However, the nature of water interference remains unknown and necessitates the pursuit of kinetic studies to clarify the colorimetric CO_2 sensing mechanism.

The ZIF-8 colorimetric sensor offers a simple detection of CO_2 via incorporation of reactions between ethylenediamine, phenolsulfonpthalein, and CO_2. Through integration of water-resistant functionalities, the MOF gas sensor will be enhanced to develop a competitive colorimetric device robust to the variable humidity characteristic of indoor air environment.

CRediT authorship contribution statement

Adrian K. Davey: Conceptualization, Data curation, Formal analysis, Funding acquisition, Investigation, Software, Validation, Writing - original draft. **Xiang Gao:** Conceptualization, Funding acquisition, Supervision, Writing - review & editing. **Yong Xia:** Investigation. **Zhou Li:** Investigation. **Matthew N. Dods:** Investigation, Resources, Writing - review & editing. **Steven Delacruz:** Investigation. **Aifei Pan:** Conceptualization. **Sanket Swamy:** Investigation. **David Gardner:** Conceptualization, Writing - review & editing. **Carlo Carraro:** Writing - review & editing. **Roya Maboudian:** Conceptualization, Funding acquisition, Project administration, Resources, Supervision, Writing - review & editing.

Declaration of Competing Interest

The authors report no declarations of interest.

Acknowledgements

The authors gratefully acknowledge the support of the National Science Foundation in the form of a Graduate Research Fellowship (A.K. D.) and grant # 1903188, as well as the Bakar Fellows Program. Work at the Molecular Foundry was supported by the Office of Science, Office of Basic Energy Sciences, of the U.S. Department of Energy under Contract No. DE-AC02-05CH11231. The contributions of M.N.D. were supported by the U.S. Department of Energy, Office of Science, Office of Basic Energy Sciences under award DE-SC0019992. The authors also thank Dr. Guangwei Min of the Electron Microscopy Laboratory (EML) at the University of California, Berkeley for advice and assistance in SEM sample preparation and image collection.

Appendix A. Supplementary data

Supplementary material related to this article can be found, in the online version, at doi:https://doi.org/10.1016/j.snb.2021.130313.

References

[1] K. Azuma, N. Kagi, U. Yanagi, H. Osawa, Effects of low-level inhalation exposure to carbon dioxide in indoor environments: a short review on human health and psychomotor performance, Environ. Int. 121 (2018) 51–56, https://doi.org/10.1016/j.envint.2018.08.059.

[2] J.G. Allen, P. MacNaughton, U. Satish, S. Santanam, J. Vallarino, J.D. Spengler, Associations of cognitive function scores with carbon dioxide, ventilation, and volatile organic compound exposures in office workers: a exposure study of green and conventional office environments, Environ. Health Perspect. 124 (2016) 805–812, https://doi.org/10.1289/ehp.1510037.

[3] M.G. Apte, W.J. Fisk, J.M. Daisey, Associations between indoor CO_2 concentrations and sick building syndrome symptoms in U.S. office buildings: an analysis of the 1994-1996 BASE study data, Indoor Air 10 (2000) 246–257, https://doi.org/10.1034/j.1600-0668.2000.010004246.x.

[4] D.H. Tsai, J.S. Lin, C.C. Chan, Office workers' sick building syndrome and carbon dioxide concentrations, J. Occup. Environ. Hyg. 9 (5) (2012) 345–351, https://doi.org/10.1080/15459624.2012.675291.

[5] U. Satish, M.J. Mendell, K. Shekhar, T. Hotchi, D. Sullivan, S. Streufert, W.J. Fisk, Is CO_2 an indoor pollutant? Direct effect of low-to-moderate concentrations on human decision-making performance, Environ. Health Perspect. 120 (12) (2012) 1671–1677, https://doi.org/10.1289/ehp.1104789.

[6] R.-Y. Chen, K.-F. Ho, T.-Y. Chang, G.-B. Hong, C.-W. Liu, K.-J. Chuang, In-vehicle carbon dioxide and adverse effects: an air filtration-based intervention study, Sci. Total Environ. 723 (2020) 138047, https://doi.org/10.1016/j.scitotenv.2020.138047.

[7] Web reference one, "Carbon Dioxide." U.S. Department of Health & Human Services, the National Institute for Occupational Safety and Health (NIOSH), Centers for Disease Control and Prevention (CDC), 2021. https://www.cdc.gov/niosh/npg/npgd0103.html.

[8] L. Kajtár, L. Herczeg, Influence of carbon-dioxide concentration on human well-being and intensity of mental work, Quart. J. Hungarian Meteorol. Service 116 (2012) 145–169.

[9] X. Jia, J. Roels, R. Baets, G. Roelkens, On-chip non-dispersive infrared CO_2 sensor on an integrating cylinder, Sensors 19 (2019) 4260, https://doi.org/10.3390/s19194260.

[10] B. Liu, J. Zhuang, G. Wei, Recent advances in the design of colorimetric sensors for environmental monitoring, Environ. Sci. Nano 7 (2020) 2195, https://doi.org/10.1039/D0EN00449A.

[11] C. Chatterjee, A. Sen, Sensitive colorimetric sensors for visual detection of carbon dioxide and sulfur dioxide, J. Mater. Chem. A 3 (2015) 5642, https://doi.org/10.1039/C4TA06321J.

[12] A. Mills, Q. Chang, N. McMurray, Equilibrium studies on colorimetric plastic film carbon dioxide, Anal. Chem. 64 (1992) 1383–1389, https://doi.org/10.1021/ac00037a015.

[13] H. Jain, C. Vargese, Use of disposable end tidal carbon dioxide detector device for checking endotracheal tube placement, J. Clin. Diagn. Res. 1 (2007) 10–16.

[14] Web reference two, NellCor™ Adult/Pediatric Colorimetric CO_2 Detector, Medtronic, 2021. https://www.medtronic.com/covidien/en-us/products/intubation/nellcor-adult-pediatric-colorimetric-co2-detector.html.

[15] L. Feng, C.J. Musto, J.W. Kemling, S.H. Lim, K.S. Suslick, A colorimetric sensor array for identification of toxic gases below permissible exposure limits, Chem. Commun. 46 (2010) 2037–2039, https://doi.org/10.1039/b926848k.

[16] S.H. Cho, J.M. Suh, T.-H. Eom, T. Kim, H.-W. Jang, Colorimetric sensors for toxic and hazardous gas detection: a review, Electron. Mater. Lett. 17 (2021) 1–17, https://doi.org/10.1007/s13391-020-00254-9.

[17] H. Furukawa, K.E. Cordova, M. O'Keeffe, O.M." Yaghi, The chemistry and applications of metal-organic frameworks, Science 341 (6149) (2013) 1230444–1–123044–12, https://doi.org/10.1126/science.1230444.

[18] A.E. Baumann, D.A. Burns, B. Liu, V.S. Thoi, Metal-organic framework functionalization and design strategies for advanced electrochemical energy

storage devices, Commun. Chem. 2 (2019) 86, https://doi.org/10.1038/s42004-019-0184-6.
[19] J.R. Long, O.M. Yaghi, The pervasive chemistry of metal-organic frameworks, Chem. Soc. Rev. 38 (2009) 1213–1214, https://doi.org/10.1039/B903811F.
[20] C. Wang, D. Liu, W. Lin, Metal-organic framework as a tunable platform for designing functional molecular materials, J. Am. Chem. Soc. 125 (2013) 13222–13234, https://doi.org/10.1021/ja308229p.
[21] W. Lu, Z. Wei, Z.Y. Gu, T.F. Liu, J. Park, J. Park, J. Tian, M. Zhang, Q. Zhang, T. Gentle, M. Bosch, H.C. Zhou, Tuning the structure and function of metal organic frameworks *via* linker design, Chem. Soc. Rev. 43 (2014) 5561, https://doi.org/10.1039/C4CS00003J.
[22] J. Lyu, X. Zhang, K. Otake, X. Wang, P. Li, Z. Li, Z. Chen, Y. Zhang, M.C. Wasson, Y. Yang, P. Bai, X. Guo, T. Islamoglu, O.K. Farha, Topology and porosity control of metal-organic frameworks through linker functionalization, Chem. Sci. 10 (2019) 1186, https://doi.org/10.1039/c8sc04220a.
[23] M. Kalaj, S.M. Cohen, Postsynthetic modification: an enabling technology for the advancement of metal-organic frameworks, ACS Cent. Sci. 6 (2020) 1046–1057, https://doi.org/10.1021/acscentsci.0c00690.
[24] E.D. Bloch, M.R. Hudson, J.A. Mason, S. Chavan, V. Crocella, J.D. Howe, K. Lee, A. L. Dzubak, W.L. Queen, J.M. Zadrozny, S.J. Geier, L.C. Lin, L. Gagliardi, B. Smit, J. B. Neaton, S. Bordiga, C.M. Brown, J.R. Long, Reversible CO binding enables tunable CO/H_2 and CO/N_2 separations in metal-organic frameworks with exposed divalent metal cations, J. Am. Chem. Soc. 136 (2014) 10752–10761, https://doi.org/10.1021/ja505318p.
[25] B.R. Barnett, M.I. Gonzalez, J.R. Long, Recent progress towards light hydrocarbon separations using metal-organic frameworks, Trends Chem. 1 (2019) 159–171, https://doi.org/10.1016/j.trechm.2019.02.012.
[26] K. Sumida, D.L. Rogow, J.A. Mason, T.M. McDonald, E.D.' Bloch, Z.R. Herm, T. H. Bae, J.R. Long, Carbon dioxide capture in metal-organic frameworks, Chem. Rev. 112 (2) (2012) 724–781, https://doi.org/10.1021/cr2003272.
[27] Z. Zhang, Z.Z. Yaho, S. Xiang, B. Chen, Perspective of microporous metal-organic frameworks for CO_2 capture and separation, Energy Environ. Sci. 7 (2014) 2868, https://doi.org/10.1039/C4EE00143E.
[28] D.W. Gardner, X. Gao, H.M. Fahad, A.-T. Yang, S. He, A. Javey, C. Carraro, R. Maboudian, Transistor-based work-function measurement of metal–organic frameworks for ultra-low-power, rationally designed chemical sensors, Chem. – Eur. J. 25 (2019) 13176–13183, https://doi.org/10.1002/chem.201902483.
[29] I. Stassen, J.H. Dou, C. Hendon, M. Dinca, Chemiresistive sensing of ambient CO_2 by an autogenously-hydrated Cu_3(hexaiminobenzene)$_2$ framework, ACS Cent. Sci. 5 (2019) 1425–1431, https://doi.org/10.1021/acscentsci.9b00482.
[30] L.S. Xie, G. Skorupskii, M. Dincă, Electrically conductive metal-organic frameworks, Chem. Rev. 120 (2020) 8536–8580, https://doi.org/10.1021/acs.chemrev.9b00766.
[31] M.C. Wasson, C.T. Buru, Z. Chen, T. Islamoglu, O.K. Farha, Metal-organic frameworks: a tunable platform to access single-site heterogenous catalysts, Appl. Catal. A Gen. 586 (2019) 117214, https://doi.org/10.1016/j.apcata.2019.117214.
[32] J.-Y. Lee, O.K. Farha, J. Roberts, K.A. Scheidt, S.-B.T. Nguyen, J.T. Hupp, Metal-organic framework materials as catalysts, Chem. Soc. Rev. 38 (2009) 1450–1459, https://doi.org/10.1039/b807080f.
[33] K.S. Park, Z. Ni, A.P. Côté, J.Y. Choi, R. Huang, F.J. Uribe-Romo, H.K. Chae, M. O'Keeffe, O.M. Yaghi, Exceptional chemical and thermal stability of zeolitic imidazolate frameworks, Proc. Natl. Acad. Sci. U. S. A. 103 (27) (2006) 10186–10191, https://doi.org/10.1073/pnas.0602439103.
[34] Y.R. Lee, M.S. Jang, H.Y. Cho, H.J. Kwon, S. Kim, W.S. Ahn, ZIF-8: a comparison of synthesis methods, Chem. Eng. J. 271 (2015) 276–280, https://doi.org/10.1016/j.cej.2015.02.094.
[35] H. Zhang, J. Hou, Y. Hu, P. Wang, R. Ou, L. Jiang, J.Z. Liu, B.D. Freeman, A.J. Hill, H. Wang, Ultrafast selective transport of alkali metal ions in metal organic frameworks with subnanometer pores, Sci. Adv. 4 (2018), https://doi.org/10.1126/sciadv.aaq0066 eaaq0066.
[36] J. Perez-Pellitero, H. Amrouche, F.R. Siperstein, G. Pirngruber, C. Nieto-Draghi, G. Chaplais, A. Simon-Masseron, D. Bazer-Bachi, D. Peralta, N. Bats, Adsorption of CO_2, CH_4, and N_2 on zeolitic imidazolate frameworks: experiments and simulations, Chem. Eur. J. 16 (2010) 1560–1571, https://doi.org/10.1002/chem.200902144.
[37] D. Liu, Y. Wu, Q. Xia, Z. Li, H. Xi, Experimental and molecular simulation studies of CO_2 adsorption on zeolitic imidazolate frameworks: ZIF-8 and amine-modified ZIF-8, Adsorption 19 (2013) 25–37, https://doi.org/10.1007/s10450-012-9407-1.
[38] L. Zhang, G. Wu, J. Jiang, Adsorption and diffusion of CO_2 and CH_4 in zeolitic imidazolate framework-8: effect of structural flexibility, J. Phys. Chem. C 118 (2014) 8788–8794, https://doi.org/10.1021/jp500796e.
[39] F.X. Coudert, Molecule mechanism of swing effect in zeolitic imidazolate framework ZIF-8: continuous deformation upon adsorption, ChemPhysChem 18 (2017) 2732–2738, https://doi.org/10.1002/cphc.201700463.
[40] S.A. Moggach, T.D. Bennett, A.K. Cheetham, The effect of pressure on ZIF-8: increasing pore size with pressure and the formation of a high-pressure phase of 1.47 GPa.**, Angew. Chem. Int. Ed. 48 (2009) 7087–7089, https://doi.org/10.1002/anie.200902643.
[41] C. Zhang, R.P. Lively, K. Zhang, J.R. Johnson, O. Karvan, W.J. Koros, Unexpected molecular sieving properties of zeolitic imidazolate Framework-8, J. Phys. Chem. Lett. 3 (16) (2012) 2130–2134, https://doi.org/10.1021/jz300855a.
[42] C.L. Hobday, C.H. Woodall, M.J. Lennox, M. Frost, K. Kamenev, T. Düren, C. A. Morrison, S.A. Moggach, Understanding the adsorption process in ZIF-8 using high pressure crystallography and computational modelling, Nat. Commun. 9 (1429) (2018) 1–9, https://doi.org/10.1038/s41467-018-03878-6.
[43] P. Küsgens, M. Rose, I. Senkovska, H. Fröde, A. Henschel, S. Siegle, S. Kaskel, Characterization of metal-organic frameworks by water adsorption, Microporous Mesoporous Mater. 120 (2009) 325–330, https://doi.org/10.1016/j.micromeso.2008.11.020.
[44] H. Yin, H. Kim, J. Choi, A.C.K. Yip, Thermal stability of ZIF-8 under oxidative and inert environments: a practical perspective on using ZIF-8 as a catalyst support, Chem. Eng. J. 278 (2015) 293–300, https://doi.org/10.1016/j.cej.2014.08.075.
[45] J.B. James, Y.S. Lin, Kinetics of ZIF-8 thermal decomposition in inert, oxidizing, and reducing environments, J. Phys. Chem. C 120 (2016) 14015–14026, https://doi.org/10.1021/acs.jpcc.6b01208.
[46] B. Ye, A. Gheorghe, R. van Hal, M. Zevenbergen, S. Tanase, CO_2 sensing under ambient conditions using metal-organic frameworks, Mol. Syst. Des. Eng. 5 (2020) 1071, https://doi.org/10.1039/D0ME00004C.
[47] J. Cravillon, S. Munzer, S.J. Lohmeier, A. Feldhoff, K. Huber, M. Wiebcke, Rapid room-temperature synthesis and characterizatin of nanocrystals of a prototypical zeolitic imidazolate framework, Chem. Mater. 21 (8) (2009) 1410–1412, https://doi.org/10.1021/cm900166h.
[48] P. Kubelka, New contributions to the optics of intensely light-scattering materials. Part I, J. Opt. Soc. Am. 38 (5) (1948) 448, https://doi.org/10.1364/JOSA.38.000448.
[49] M.L. Myrick, M.N. Simcock, M. Baranowski, H. Brooke, S.L. Morgan, J. N. McCutcheon, The Kubelka-Munk diffuse reflectance formula revisited, Appl. Spectrosc. Rev. 46 (2011) 140–165, https://doi.org/10.1080/05704928.2010.537004.
[50] R.A. de la Osa, I. Iparragirre, D. Ortiz, J.M. Saiz, The extended Kubelka-Munk theory and its application to spectroscopy, ChemTexts 6 (2) (2020) 1–14, https://doi.org/10.1007/s40828-019-0097-0.
[51] W.E. Vargas, G.A. Niklasson, Applicability conditions of the Kubelka-Munk theory, Appl. Opt. 36 (22) (1997) 5580–5586, https://doi.org/10.1364/AO.36.005580.
[52] B. Kruse, Li. Yang, Revised Kubelka-Munk theory. I. Theory and application, J. Opt. Soc. Am. A 21 (10) (2004) 1933–1941, https://doi.org/10.1364/JOSAA.21.001933.
[53] Web reference three, What Is Kubelka-Munk? Harrick Scientific Products, Inc., 2021. https://mmrc.caltech.edu/FTIR/Literature/Diff%20Refectance/Kubelka-Munk.pdf.
[54] C. Luis, Y. Castaño-Guerrero, R. Soares, G. Sales, R. Fernandes, Avoiding the interference of doxorubicin with MTT measurements on the MCF-7 breast cancer cell line, Methods Protoc. 2 (2019) 29, https://doi.org/10.3390/mps2020029.
[55] Web reference four, CSD Single Crystal Ccdc VELVOY, CCDC, 2021, p. 602542, https://www.ccdc.cam.ac.uk/structures/search?identifier=VELVOY (Accessed 2020/1/18).
[56] Y. Zhang, Y. Jia, M. Li, L. Hou, Influence of the 2-methylimidazole/zinc nitrate hexahydrate molar ratio on the synthesis of zeolitic imidazolate framework-8 crystals at room temperature, Sci. Rep. 8 (2018), 9597, https://doi.org/10.1038/s41598-018-28015-7.
[57] M. Ding, X. Cai, H.-L. Jiang, Improving MOF stability: approaches and applications, Chem. Sci. 10 (2019) 10209, https://doi.org/10.1039/c9sc03916c.
[58] M. Bosch, M. Zhang, H.-C. Zhou, Increasing the stability of metal-organic frameworks, Adv. Chem. (2014) 182327, https://doi.org/10.1155/2014/182327.
[59] D.N. Ta, H.K.D. Nguyen, B.X. Trinh, Q.T.N. Le, H.N. Ta, H.T. Nguyen, Preparation of nano-ZIF-8 in methanol with high yield, Can. J. Chem. Eng. 96 (2018) 1518–1530, https://doi.org/10.1002/cjce.23155.
[60] C. Avci, A. Yazdi, M. Tarres, E. Bernoud, N.G. Bastus, V. Puntes, I. Imaz, X. Ribas, D. Maspoch, Sequential deconstruction—reconstruction of metal-organic frameworks: an alternative strategy for synthesizing (multi)-layered ZIF composites, ACS Appl. Mater. Interfaces 10 (2018) 23952–23960, https://doi.org/10.1021/acsami.8b05098.
[61] M. Yahia, Q.N. Phan Le, N. Ismail, M. Essalhi, O. Sundman, A. Rahimpour, M. M. Dal-Cin, N. ad Tavajohi, Effect of incorporating different ZIF-8 crystal sizes in the polymer of intrinsic microporosity, PIM-1, for CO_2, Microporous Mesoporous Mater. 312 (2021) 110761, https://doi.org/10.1016/j.micromeso.2020.110761.
[62] Indoor Air Quality (IAQ), Volatile Organic Compounds' Impact on Indoor Air Quality, United States Environmental Protection Agency (EPA), 2021. https://www.epa.gov/indoor-air-quality-iaq/volatile-organic-compounds-impact-indoor-air-quality#Levels.
[63] Toxic Substances Portal: Public Health Statement for Acetone, Agency for Toxic Substances and Disease Registry, 2015 https://wwwn.cdc.gov/TSP/PHS/PHS.aspx?phsid=3&toxid=1#:~:text=The%20typical%20level%20of%20acetone,8%20ppb%20versus%207%20ppb. (Accessed 2021/6/08).
[64] Indoor Air Quality (IAQ): Carbon Monoxide's Impact on Indoor Air Quality, United States Environmental Protection Agency (EPA), 2020 https://www.epa.gov/indoor-air-quality-iaq/carbon-monoxides-impact-indoor-air-quality#:~:text=Average%20levels%20in%20homes%20without,be%2030%20ppm%20or%20higher. (Accessed 2021/6/08).
[65] Using Phenol Red to Assess pH in Tissue Culture Media. Using the Cytation 5 Cell Imaging Microplate Reader to Monitor Cell Culture, Biotek, 2018 https://www.biotek.com/resources/application-notes/using-phenol-red-to-assess-ph-in-tissue-culture-media/ (Accessed 2020/9/20).
[66] Z. Zhang, S. Xian, Q. Xia, H. Wang, Z. Li, J. Li, Enhancements of CO_2 adsorption and CO_2/N_2 selectivity on ZIF-8 via postsynthetic modification, AIChE 59 (6) (2013) 2195–2206, https://doi.org/10.1002/aic.13970.
[67] M. Caplow, Kinetics of carbamate formation and breakdown, J. Am. Chem. Soc. 90 (24) (1968) 6795–6803, https://doi.org/10.1021/ja01026a041.
[68] P.V. Danckwerts, The reaction of CO_2 with ethanolamines, Chem. Eng. Sci. 34 (1979) 443–446, https://doi.org/10.1016/0009-2509(79)85087-3.

[69] E. Sada, H. Kumazawa, Z.Q. Han, Kinetics of reaction between carbon dioxide and ethylenediamine in nonaqueous solvents, Chem. Eng. J. 31 (1985) 109–115, https://doi.org/10.1016/0300-9467(85)80049-6.
[70] E. Sada, H. Kumazawa, Y. Osawa, M. Matsuura, Z.Q. Han, Reaction kinetics of carbon dioxide with amines in non-aqueous solvents, Chem. Eng. J. 33 (1986) 87–95, https://doi.org/10.1016/0300-9467(86)80038-7.
[71] R.J. Littel, G.F.' Versteeg, W.P.M. Van Swaaij, Kinetics of CO_2 with primary and secondary amines in aqueous solutions – I. Zwitterion deprotonation kinetics for DEA and DIPA in aqueous blends of alkanolamines, Chem. Eng. Sci. 47 (3) (1992) 2027–2035, https://doi.org/10.1016/0009-2509(92)80319-8.
[72] G. Couchax, D. Barth, M. Jacquin, A. Faraj, J. Grandjean, Kinetics of carbon dioxide with amines. I. Stopped-flow studies in aqueous solutions. A review, Oil Gas Sci. Technol. – Rev. IFP Energies Nouvelles 69 (5) (2014) 865–884, https://doi.org/10.2516/ogst/2013150.
[73] J. Wesierska-Gadek, T. Schreiner, M. Maurer, A. Waringer, C. Ranftler, Phenol red in the culture medium strongly affects the susceptibility of human MFC-7 cells to roscovitine, Cell. Mol. Biol. Lett. 12 (2007) 280–293, https://doi.org/10.2478/s11658-007-0002-5.
[74] J.J. Gassensmith, H. Furukawa, R.A. Smaldone, R.S. Forgan, Y.Y. Botros, O. M. Yaghi, J.F. Stoddart, Strong and reversible binding of carbon dioxide in a green metal-organic framework, J. Am. Chem. Soc. 133 (2011) 15312–15315, https://doi.org/10.1021/ja206525x.
[75] H. Karlsson, H. Svensson, Rate of absorption of CO_2 absorption systems using a wetted wall column, Energy Procedia 114 (2017) 2009–2023, https://doi.org/10.1016/j.egypro.2017.03.1335.
[76] S. Moioili a, L.A. Pellegrini, S. Gamba, Simulation of CO_2 capture by MEA scrubbing with a rate-based model, Procedia Eng. 42 (2012) 1651–1661, https://doi.org/10.1016/j.proeng.2012.07.558.
[77] D.S. Mebane, J.D. Kress, C.B. Storlie, D.J. Fauth, M.L. Gray, K. Li, Transport, zwitterions, and the role of water of CO_2 mesoporous silica-supported amine sorbents, J. Phys. Chem. C 117 (2013) 26617–26627, https://doi.org/10.1021/jp4076417.
[78] R. Ben Said, J.M. Koelle, K. Essalah, B. Tangour, A. Sayari, Unified approach to CO_2-amine reaction mechanisms, ACS Omega 5 (2020) 26125–26133, https://doi.org/10.1021/acsomega.0c03727.
[79] E.F.' da Silva, H.F. Svendsen, Ab initio study of the reaction of carbamate formation and alkanolamines, Ind. Eng. Chem. Res. 43 (2004) 3413–3418, https://doi.org/10.1021/ie030619k.
[80] J.E. Crooks, J.P. Donnellan, Kinetics and mechanism of the reaction between carbon dioxide and amines in aqueous solution, J. Chem. Perkin Trans. 2 (44) (1989) 331–333, https://doi.org/10.1039/P29890000331.
[81] P.D. Vaidya, E.Y. Kenig, Termolecular kinetic model for CO_2-alkanolamine reactions: an overview, Chem. Eng. Technol. 33 (10) (2010) 1577–1581, https://doi.org/10.1002/ceat.201000050.
[82] H.-B. Xie, Y. Zhou, Y. Zhang, J.K. Johnson, Reaction mechanism of monoethanolamine with CO_2 in aqueous solution from molecular modeling, J. Phys. Chem. A 114 (2010) 11844–11852, https://doi.org/10.1021/jp107516k.
[83] R.W. Flaig, T.M. Obsorn Popp, A.M. Fracaroli, E.A. Kapustin, M.J. Kalmutzski, R. M. Atamimi, F. Fathieh, J.A. Reimer, O.M. Yaghi, The chemistry of CO_2 capture in an amine-functionalized metal-organic framework under dry and humid conditions, J. Am. Chem. Soc. 139 (2017) 12125–12128, https://doi.org/10.1021/jacs.7b06382.
[84] G.F. Versteeg, L.A.J. Van Dijck, W.P.M. Van Swaaij, On the kinetics between CO_2 and alkanolamines both in aqueous and nonaqueous solutions. An overview, Chem. Eng. Commun. 144 (1996) 113–158, https://doi.org/10.1080/00986449608936450.
[85] P.D. Vaidya, E.Y. Kenig, CO_2-alkanolamine reaction kinetics: a review of recent studies, Chem. Eng. Technol. 30 (11) (2007) 1467–1474, https://doi.org/10.1002/ceat.200700268.
[86] A. Aboudheir, P. Tontiwachwuthikul, A. Chakma, R. Idem, Novel design for the nozzle of a laminar jet absorber, Ind. Eng. Chem. Res. 43 (2004) 2568–2574, https://doi.org/10.1021/ie0341606.
[87] P.D. Vaidya, V.V. Mahajani, Kinetics of the reaction of CO_2 with aqueous formulated solution containing monoethanolamine, N-methyl-2-pyrrolidone, and diethylene glycol, Ind. Eng. Chem. Res. 44 (2005) 1868–1873, https://doi.org/10.1021/ie049226r.
[88] A. Aboudheir, P. Tontiwachwuthikul, A. Chakma, R. Idem, Kinetics of the reactive absorption of carbon dioxide in high CO_2-loaded, concentrated aqueous monoethanolamine solutions, Chem. Eng. Sci. 58 (2003) 5195–5210, https://doi.org/10.1016/j.ces.2003.08.014.
[89] H. Zhang, R.Q. Snurr, Computational study of water adsorption in the hydrophobic metal-organic framework ZIF-8: adsorption mechanism and acceleration of the simulations, J. Phys. Chem. C 121 (43) (2017) 24000–24010, https://doi.org/10.1021/acs.jpcc.7b06405.
[90] M. Gao, J. Wang, Z. Rong, Q. Shi, J. Dong, A combined experimental-computational investigation on water adsorption in various ZIFs with the SOD and RHO topologies, RSC Adv. 8 (2018) 39627, https://doi.org/10.1039/C8RA08460B.
[91] J. Pokhrel, N. Bhoria, S. Anastasiou, T. Tsoufis, D. Gournis, G. Romanos, G. N. Karanikolos, CO_2adsorption behavior of amine-functionalized ZIF-8, Microporous Mesoporous Mater. 267 (2018) 53–67, https://doi.org/10.1016/j.micromeso.2018.03.012.
[92] S.A. Didas, A.R.' Kulkarni, D.S. Sholl, C.W. Jones, Role of amine structure on carbon dioxide adsorption from ultradilute gas streams such as ambient air, ChemSusChem 5 (2012) 2058–2064, https://doi.org/10.1002/cssc.201200196.
[93] C. Lin, X. Xian, X. Qin, D. Wang, F. Tsow, E. Forzani, N. Tao, High performance colorimetric carbon monoxide sensor for continuous personal exposure monitoring, ACS Sens. 3 (2018) 327–333, https://doi.org/10.1021/acssensors.7b00722.
[94] J. Yu, D. Wang, V.V. Tipparaju, F. Tsow, X. Xian, Mitigation of humidity interference in colorimetric sensors, ACS Sens. 6 (2021) 303–320, https://doi.org/10.1021/acssensors.0c01644.
[95] X. Liu, Y. Li, Y. Ban, Y. Peng, H. Jin, H. Bux, L. Xu, J. Caro, W. Yang, Improvement of hydrothermal stability of zeolitic imidazolate frameworks, Chem. Commun. 49 (2013) 9140, https://doi.org/10.1039/C3CC45308A.

Adrian K. Davey is currently pursuing a Ph.D. in Chemical & Biomolecular Engineering at the University of California, Berkeley. His research interests are in metal-organic framework-based colorimetric gas sensing.

Xiang Gao earned his Ph.D. in Chemistry from the University of California, Berkeley in 2019. His research interests are in the controlled synthesis and applications of nanomaterials enabled by metal-organic frameworks.

Yong Xia is currently pursuing a Ph.D. in Instrument Science and Technology at Xi'an Jiaotong University. His research interests are in developing new methodologies for improving the selectivity and sensitivity of gas sensors.

Zhou Li is currently pursuing a Ph.D. in Safety Science and Technology at the University of Science and Technology of China. His research interests involve the synthesis of graphene aerogel-based materials with applications in devices such as gas sensors and supercapacitors.

Matthew N. Dods is currently pursuing a Ph.D. in Chemical & Biomolecular Engineering at the University of California, Berkeley. His research interests are in developing and characterizing ultra-porous adsorbents for gas separation applications.

Steven Delacruz earned his Ph.D. in Chemical & Biomolecular Engineering from the University of California, Berkeley in 2020. His research involved silicon carbide materials and processing for energy applications as well as porous materials for chemical sensing.

Aifei Pan is currently pursuing a Ph.D. in Mechanical Engineering at Xi'an Jiaotong University. Her research interests are in computational approaches to understand the behavior of various gas sensors.

Sanket Swamy earned his Bachelor of Science in Chemical & Biomolecular Engineering from the University of California, Berkeley in 2020. His research involved colorimetric gas sensing.

David Gardner is currently pursuing a Ph.D. in Chemical & Biomolecular Engineering at the University of California, Berkeley. His research interests are in understanding materials under chemical and mechanical stimuli.

Carlo Carraro is an Adjunct Professor of Chemical & Biomolecular Engineering at the University of California, Berkeley. His research interests are in surface science, nanometrology, and microsystems technology.

Roya Maboudian is a Professor of Chemical & Biomolecular Engineering at the University of California, Berkeley and Co-Director of the Berkeley Sensor and Actuator Center (BSAC). Her research interest is in the surface/interface and materials science and engineering of micro/nanosystems, with applications in harsh-environment sensing, health and environmental monitoring, and energy technologies.